This is an author produced version of *Intersubband terahertz lasers using four-level asymmetric quantum wells* .

Article:

Intersubband terahertz lasers using four-level asymmetric quantum wells

P. Kinsler,[a] P. Harrison, and R. W. Kelsall

*Institute of Microwaves and Photonics, School of Electronic and Electrical Engineering,
University of Leeds, LS2 9JT, United Kingdom*

We demonstrate the potential for laser operation at far-infrared wavelengths (30–300 μm, 1–10 THz) by using intersubband emission in four-level GaAs/AlGaAs asymmetric (stepped) quantum wells. Achieving population inversion in these devices depends critically on the lifetimes of the nonradiative intersubband transitions, and so we have performed detailed calculations of electron–electron and electron–phonon scattering rates. Our four-subband structures show potential for the realization of room temperature lasing, unlike previously considered three-subband structures which did not give population inversions except at impractically low electron densities and temperatures. Auger-type electron–electron interactions involving the highly populated ground subband effectively destroyed the population inversion in three level systems, but in these four subband structures the inversion is maintained by strong phonon-mediated depopulation of the lower laser level. The largest population inversions are calculated at low temperatures ($<$30 K), but for the structures with higher emission energies, room temperature (300 K) operation is also predicted. © *1999 American Institute of Physics.* [S0021-8979(99)07501-5]

I. INTRODUCTION

There are numerous possible applications in both imaging and wireless communications for a compact solid-state source of terahertz radiation. The use of asymmetric or stepped quantum well structures for producing terahertz radiation from intersubband transitions was first suggested by Berger.[1] To make a successful laser using these structures we need both high quantum efficiency and a population inversion. The quantum efficiency of these devices can be improved by growing a stack of multiple active regions (i.e., multiple quantum wells). However, the population inversion needs a careful design which tunes the relaxation rates from the lasing levels, to ensure that the depopulation of the lower laser level is significantly faster than the competing repopulation from the upper laser level. Although optical pumping is less convenient than electrical injection for commercial applications, we consider optically excited structures[2,3] because it allows great simplifications in device design and fabrication.

Following Berger, later work[4] analyzed the lasing potential by designing structures based around the scattering of electrons by longitudinal-optical (LO) phonons. That work considered the effect of electron–LO-phonon scattering on the population inversion between the two emitter levels. The next step was to determine the effect of electron–electron scattering for three-subband structures, including Pauli exclusion and exchange effects, as well as the Auger-type electron–electron scattering processes caused by the asymmetry of the quantum well structures.[5] This showed that Auger-type electron–electron scattering between the upper and lower laser levels destroyed the possibility of population

inversion except at low electron densities (10^{10} cm^{-2}) and low temperatures.

Here we study a range of four-subband prototype devices which consist of a GaAs deep well layer of various widths, combined with an adjacent $Ga_{1-x}Al_xAs$ step between thick $Ga_{0.76}Al_{0.24}As$ barriers[4] (see Fig. 1 and Tables I and II). We assume an electron density of 50×10^{10} cm^{-2}. Optical pumping with a 10.6-μm-CO$_2$ laser is taken as the means to excite electrons from the lowest energy (ground) subband $|1\rangle$ to the highest subband $|4\rangle$; the aim being to create a population inversion between the fourth $|4\rangle$ and the third subband $|3\rangle$. The separation of these two subbands is designed for terahertz emission. The presence of the subband $|2\rangle$ between subband $|3\rangle$ and the ground subband $|1\rangle$ allows optimization of the phonon scattering rate out of subband $|3\rangle$ by ''resonant'' transitions (those with near zero phonon momentum).[4]
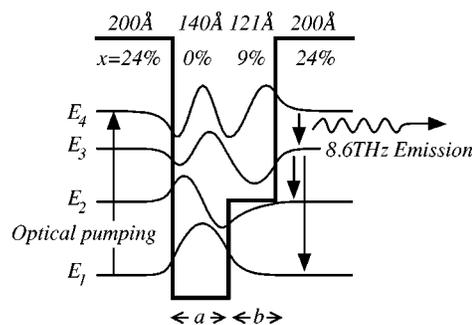

FIG. 1. Diagram of the energy levels and wave functions of a four level asymmetric quantum well (resonant prototype R_7). The energy spacing E_4-E_1 between subband $|4\rangle$ and subband $|1\rangle$ is tuned for CO$_2$ pumping, and terahertz emission is sought from the $|4\rangle$ to $|3\rangle$ transition (9.0 THz in this diagram).

a)Electronic mail: p.kinsler@elec-eng.leeds.ac.uk

TABLE I. Standard prototypes: Structural parameters of four-subband asymmetric quantum wells with a terahertz E_4-E_3 intersubband separation, with E_3-E_2 swept through the LO-phonon energy.

Label	E_4-E_3(THz)	Step x_b (%)	Step width b (Å)	E_4-E_1(meV)	E_4-E_3(meV)	E_3-E_2(meV)
S_1	11.1	6	102	116.811	45.872	32.396
S_2	10.4	7	107	116.939	42.838	33.435
S_3	9.5	8	113	117.112	39.379	35.297
S_4	9.0	8.5	117	117.002	37.414	36.372
S_5	8.6	9	121	117.069	35.420	37.728
S_6	7.5	10	131	117.079	31.139	40.769
S_7	6.4	11	145	116.880	26.478	44.234

Calculations have been done for two sets of four-subband asymmetric quantum well structures (''standard'' and ''resonant,'' as defined below), whose designs were optimized around the important electron–LO-phonon scattering processes. The potential for laser operation was estimated using the population ratio τ_{43}/τ_{3x} as defined by a simple rate equation in the steady state. This is valid below threshold, where the radiative scattering rates are still much less than the electron–electron and electron–phonon intersubband rates. Here τ_{43} is the total nonradiative lifetime for electrons scattering from the fourth $|4\rangle$ to the third subband $|3\rangle$, and τ_{3x} is the total nonradiative lifetime for electrons in the third subband $|3\rangle$ scattering down to the second or ground ($|2\rangle$ or $|1\rangle$) subbands.

The methods we use are described in more detail in an earlier paper,[5] but for convenience we include a brief summary here. The energy levels and wave functions of the quantum wells were obtained by numerical solution of the effective mass Schrödinger equation.[6] The electronic dispersions are assumed to be parabolic. The population distributions of electrons and phonons were described by Fermi–Dirac and Bose–Einstein distributions, respectively, and it was assumed that both electron and phonon temperatures for any electron subband or phonon type were the same as the lattice temperature. The use of Fermi–Dirac electron distributions is not unreasonable, since intrasubband electron–electron scattering is much faster than intersubband scattering, so the electron distributions thermalize rapidly. Although the distribution of electrons in the upper subbands might be characterized by their own ''electron temperature,'' these could only be obtained by a self-consistent solution of the Boltzmann transport equation, something which is beyond the scope of this article. The numerical wave functions were then used to calculate scattering rates using Fermi's golden rule.[7] The electron–phonon scattering rates included

the acoustic (deformation potential) and polar-LO phonon interactions. We use bulklike phonon modes, since recent calculations of electron–phonon scattering in asymmetric quantum wells using localized phonon modes[8,9] show that the population ratios calculated by either the bulk-phonon or localized-phonon approach are comparable, despite the fact that the phonon potentials differ markedly in the two cases. We denote electron–phonon scattering events with two indices ''phij,'' where i is the initial subband of the electron, and j is its final subband. Electron–electron scattering events[10–12] are denoted using the indices ''$ijfg$,'' where i and j are the subbands of the initial electron states, and f and g are the subbands of the final electron states. For events where the final state is any subband lower in energy we use the subscript x, e.g., ph$3x$ is both ph32 and ph31. We assume identical distributions and equal densities for both spin up and spin down electrons and use a temperature dependent dielectric function.[13,14]

The article is organized as follows: in Sec. II we show the results for a set of ''standard'' prototypes in which the subband energy separation E_3-E_2 is swept through the LO-phonon energy; in Sec. III we look at a set of ''resonant'' prototypes in which the subband energy separation E_3-E_2 is always resonant with the LO-phonon energy in order to maximize the depopulation of the lower laser subband; and finally in Sec. IV we present our conclusions.

II. STANDARD PROTOTYPES

The first set of four-subband prototypes (Table I) is designed for a range of THz emission energies. They consist of two 200 Å Al$_{0.24}$Ga$_{0.76}$As barriers which surround a 65 Å GaAs well layer and a bÅ Al$_{x_b}$Ga$_{1-x_b}$As step layer. The effect of depopulation of the lower laser subband $|3\rangle$ by electron–LO-phonon scattering is tested by sweeping E_3

TABLE II. Resonant prototypes: Structural parameters of four-subband asymmetric quantum wells satisfying the resonant depopulation criterion $E_3-E_2=E_{LO}$.

Label	E_4-E_3(THz)	a (Å)	b (Å)	x_b (%)	E_4-E_3 (meV)	E_3-E_2 (meV)
R_1	11.8	40	179	10	48.910	35.829
R_2	10.7	80	149	6	44.366	35.375
R_3	11.7	90	136	4	48.557	37.373
R_4	0.6	100	700	17	2.628	36.734
R_5	5.1	120	220	13	20.965	37.244
R_6	7.2	130	163	11	29.612	36.722
R_7	9.0	140	117	8.5	37.414	36.372

FIG. 3. Predicted population ratios for the standard prototypes listed in Table I. The electron densities in the subbands are $n_1 = 47 \times 10^{10}$ cm^{-2}, and $n_2 = n_3 = n_4 = 10^{10}$ cm^{-2}. Results for a range of temperatures are shown by different lines.
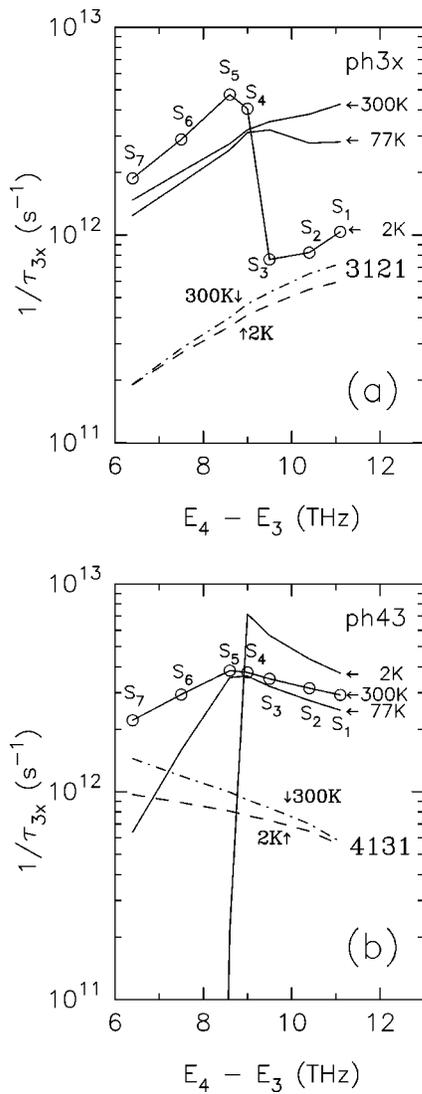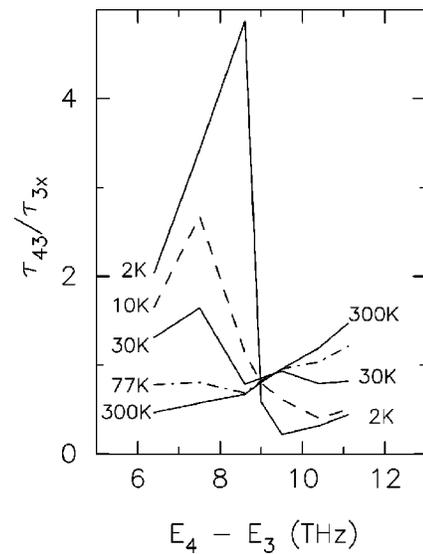

FIG. 2. A comparison of the total scattering rates between subbands for the standard prototypes listed in Table I. The electron densities in the subbands are $n_1 = 47 \times 10^{10}$ cm^{-2}, and $n_2 = n_3 = n_4 = 10^{10}$ cm^{-2}. (a) The summed $|3\rangle \rightarrow |2\rangle$ and $|3\rangle \rightarrow |1\rangle$ electron–phonon scattering rate (''ph3x;'' solid lines; for 2, 77, and 300 K), and its complementary electron–electron scattering rate (''3121;'' dashed line is 2 K, dotted-dashed is 300 K). (b) The $|4\rangle \rightarrow |3\rangle$ electron–phonon rate (''ph43;'' solid lines; for 2, 77, and 300 K), and its complementary electron–electron scattering rate (''4131;'' dashed line is 2 K, dotted-dashed is 300 K).

$-E_2$ through the LO-phonon energy by varying the step width and composition. The aim is to depopulate the lower laser subband $|3\rangle$ faster than it is being repopulated from the upper laser subband $|4\rangle$, thus creating a population inversion between the two subbands. The ground-state subband $|1\rangle$ acts as a source of carriers for the pumping process, and a sink for the depopulation of the lower laser subband. The structures have been previously analyzed considering only the electron–phonon scattering rates,[4] and this predicted that a population ratio greater than 1 might be achieved at room temperature (300 K).

The main scattering processes that depopulate the lower laser subband ($|3\rangle \rightarrow |2\rangle, |1\rangle$) with the total rate of $1/\tau_{3x}$ are temperature dependent, as can be seen on Fig. 2(a). For prototypes which have subband separations $E_3 - E_2$ greater than

the LO-phonon energy E_{LO} (see Table I), the depopulation rate is almost completely due to the electron–LO-phonon scattering processes (''ph3x''), and is faster at 2 K than 300 K. For $E_3 - E_2 < E_{LO}$, the reverse occurs as the dominant $|3\rangle \rightarrow |2\rangle$ electron–LO-phonon scattering process presently needs to rely on thermally excited electrons which have enough energy to emit an LO-phonon and drop into the $|2\rangle$ subband. The proportion of sufficiently excited electrons increases with temperature, and therefore so does the ph32 contribution to the scattering rate $1/\tau_{32}$. The 3121 electron–electron scattering process provides an additional contribution which is not necessarily negligible, since at low temperatures it becomes comparable to the combined phonon rates. This contribution from the 3121 process increases with temperature because the energy difference between an electron initially in the third subband and a thermally excited electron in the ground subband is more likely to be smaller as the temperature increases, and a smaller energy separation increases the scattering probability.

Figure 2(b) shows the $|4\rangle \rightarrow |3\rangle$ scattering rate ($1/\tau_{43}$) behaving in the opposite way to the $|3\rangle \rightarrow |2\rangle$ rate, which is expected since the $E_4 - E_3$ separation decreases as $E_3 - E_2$ increases. The LO-phonon scattering contribution from the ph43 process cuts off as $E_4 - E_3$ drops below the LO-phonon energy in the same way as the ph32 contribution to the scattering rate $1/\tau_{3x}$ does when $E_3 - E_2 < E_{LO}$. However, here the cutoff is more marked because there are no other contributions to ph43, unlike for ph3x which included both ph32 and ph31. Consequently, for small subband separations $E_4 - E_3$ and lower temperatures, the 4131 electron–electron scattering process *dominates* the depopulation of the upper laser subband, and so strongly affects the population ratio. Note that the 4131 process increases with temperature for the same reasons as the 3121 does.

We can see in Fig. 3 that the interplay of the $1/\tau_{43}$ and $1/\tau_{3x}$ rates leaves a region with lasing potential in the 6–9
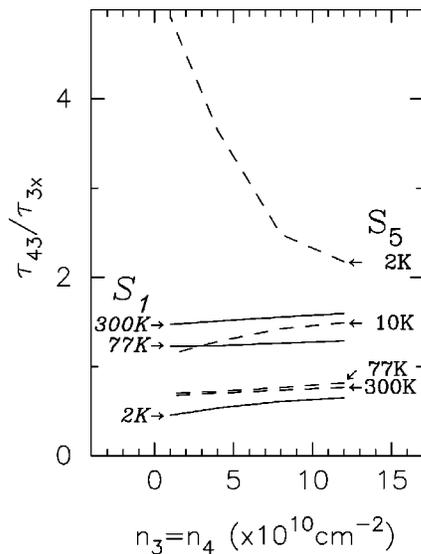
FIG. 4. Predicted population ratios for the S_5 (8.6 THz) and S_1 (11.1 THz) prototypes listed in Table I. The electron densities are $\Sigma n_i = 50 \times 10^{10}$ cm^{-2}, and $n_2 = n_3 = n_4$. The dashed lines with nonitalic labels are for the S_5 prototype at a range of temperatures (2, 10, 77, and 300 K). The solid lines with italic labels are for the ''room temperature'' S_1 prototype at a range of temperatures (2, 77, and 300 K).

THz range where a population ratio greater than 1 is most easily achieved. This is suppressed at smaller emission energies ($E_4 - E_3$) by the rapidly increasing 4131 rate, and at larger emission energies by the cutoff in the ph32 LO-phonon rate. The lasing potential reduces for higher temperatures because thermally assisted electron–LO-phonon scattering increases the $1/\tau_{43}$ rate and so suppresses the population ratio.

More surprisingly, we see an *increase* in population ratio with temperature at emission energies greater than 9 THz, where the main peak in the population ratio has been suppressed. Although only relatively modest population ratios are attainable (up to ~1.5), at 77 and 300 K they are clearly greater than 1. This occurs because the $E_3 - E_2$ separation is small, and as the temperature increases more thermally excited electrons in the lower laser level can undergo LO-phonon emission. As a result the depopulation rate $1/\tau_{3x}$ increases strongly with temperature. In contrast, $E_4 - E_3$ is large, so the $|4\rangle \rightarrow |3\rangle$ rates $1/\tau_{43}$ are only weakly dependent to the temperature. This combination leads to a net positive effect on the population ratio at higher temperatures. This offers the possibility of room temperature lasing if the potential difficulties caused by the smaller predicted population ratios can be overcome.

Figure 4 shows how the predicted population ratios of the most promising prototypes (i.e., those with the greatest population ratios at a given temperature) would change with increasing optical excitation, which would in turn increase the proportion of electrons in the upper subbands $|2\rangle, |3\rangle, |4\rangle$. For the S_5 (8.6 THz) structure (nonitalic labels, dashed lines), which performs best at low temperatures, we see a rather mixed behavior. At the lowest temperature, we see that higher laser-subband populations (with associated depletion of the ground state subband) have an adverse effect on

the predicted population ratio, but for the higher temperatures there is a weak trend in the opposite direction. In contrast, for the S_1 (11.1 THz) ''room temperature'' structure (italic labels, solid lines), which has a predicted population ratio greater than 1 at 300 K, we see that the redistribution of the electron populations has little effect on the predicted population ratio.

III. RESONANT PROTOTYPES

In the resonant prototypes (Table II) we relax the structural constraint (used in Sec. II) on the well width a and allow it to vary. This enables us to sweep $E_4 - E_3$ through the THz range while ensuring $E_3 - E_2$ is held at the LO-phonon energy. This second condition is intended to increase the probability of scattering out of the third subband since the subband separation is equal to the LO-phonon energy. As a result we do not see the cut-off in LO-phonon scattering rates at smaller $E_3 - E_2$ that occurs in the standard prototypes.

From Fig. 5 we can see that the main scattering processes that depopulate the lower laser subband ($|3\rangle \rightarrow |2\rangle, |1\rangle$) with rate $1/\tau_{3x}$ are dominated primarily by electron–LO-phonon scattering, as expected from the resonance condition used in the design.[15] The scattering rates are strongly affected by the changes in the electron wave functions for different structures, as can be seen by the abrupt changes for different $E_4 - E_3$ in Fig. 5. The $|4\rangle \rightarrow |3\rangle$ LO-phonon scattering rate has the expected temperature dependent cutoff below the LO-phonon energy. The $|3\rangle \rightarrow |2\rangle$ and $|4\rangle \rightarrow |3\rangle$ electron–electron interactions are dominated by the 3121 and 4131 processes, respectively. The 4131 electron–electron scattering rate increases markedly for $E_4 - E_3$ below 5 THz. In Fig. 6 we see the population ratios for the range of prototypes and temperatures: the largest population ratio is generated by the R_6 (7.2 THz) prototype, but another (smaller) peak occurs for the R_3 (11.7 THz) prototype for a wider range of temperatures.

We can achieve population ratios greater than 1 for low temperatures (below 50 K) in the mid-THz region, with the R_6 (7.2 THz) prototype giving the best results. The dip at 9 THz is due to the $|4\rangle \rightarrow |3\rangle$ transition coming onto resonance with the LO-phonon energy, which causes a dramatic increase in the $|4\rangle \rightarrow |3\rangle$ rate ($1/\tau_{43}$). Unlike the standard prototypes, for none of the emission energies does electron–electron scattering help the population ratio: rather, the main effect of this process is at small $E_4 - E_3$ where the proximity of the two subbands enhances the $|4\rangle \rightarrow |3\rangle$ scattering rate, thus significantly suppressing the population ratio. The R_3 (11.7 THz) prototype (italic labels, solid lines), in addition to the other prototypes emitting above 10 THz, has predicted population ratios greater than 1 for higher temperatures. The population ratios for the R_3 (11.7 THz) prototype are smaller than for R_6 (7.2 THz), but have the remarkable property that they *improve* for higher temperatures, in a similar way to that found for the 9.5–11.1 THz standard prototypes.

The most promising design for lasing is the R_6 (7.2 THz) prototype (non-italic labels, dashed lines), which at 2 K has a maximum population ratio of 4. Figure 7 shows how its
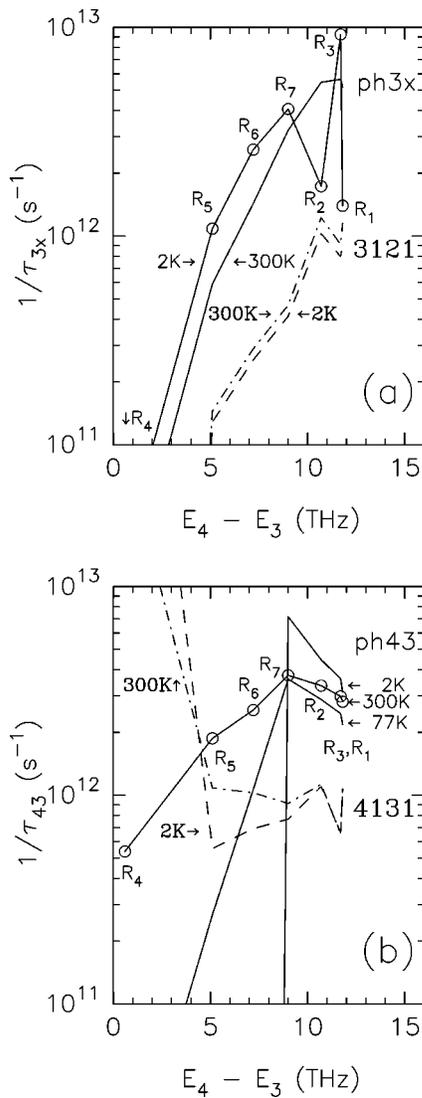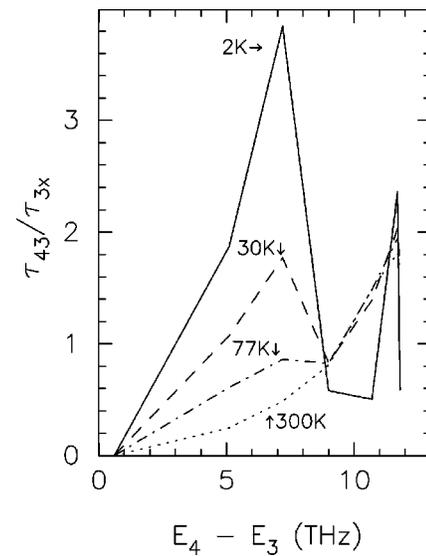
FIG. 6. Predicted population ratios for the resonant prototypes listed in Table II. The electron densities in the subbands are $n_1 = 47 \times 10^{10}$ cm^{-2}, and $n_2 = n_3 = n_4 = 10^{10}$ cm^{-2}. Results for a range of temperatures are shown by the different lines.

done on the basis of their numerically calculated "population ratio" which depends on the ratio of the intersubband scattering rates – notably the $|4\rangle \rightarrow |3\rangle$ rate ($1/\tau_{43}$) between the two laser levels, and the $|3\rangle \rightarrow |2\rangle, |1\rangle$ depopulation rate ($1/\tau_{3x}$) out of the lower laser level. Although the population ratio does depend on a number of approximations, here it serves as a useful indicator of the likelihood of achieving population inversion. These four-subband asymmetric quantum well prototypes can achieve population ratios greater than 1 with electron densities of 10^{12} cm^{-2}, unlike similar three-subband structures.[5] The main reason for this improve-

FIG. 5. A comparison of the total scattering rates between subbands for the resonant prototypes listed in Table II. The electron densities in the subbands are $n_1 = 47 \times 10^{10}$ cm^{-2}, and $n_2 = n_3 = n_4 = 10^{10}$ cm^{-2}. (a) The summed $|3\rangle \rightarrow |2\rangle$ and $|3\rangle \rightarrow |1\rangle$ electron–phonon scattering rate ("ph3x;" solid lines; for 2, 77, and 300 K), and its complementary electron–electron scattering rate ("3121;" dashed line is 2 K, dotted-dashed is 300 K). (b) The $|4\rangle \rightarrow |3\rangle$ electron–phonon rate ("ph43;" solid lines; for 2, 77, and 300 K), and its complementary electron–electron scattering rate ("4131;" dashed line is 2 K, dotted-dashed is 300 K).

population ratio varies with redistribution of electrons between the subbands. This redistribution of the electrons is intended to simulate the effects of stronger optical excitation. Clearly, the R_6 (7.2 THz) prototype works best at low temperatures with the upper levels only slightly populated. For the R_3 (11.7 THz) prototype (italic labels, solid lines), we can see that a more even distribution of carriers between the subbands only changes the population ratio slightly. This suggests that the operation of a real device based on this design would be relatively insensitive to variations in electron distribution.

IV. CONCLUSIONS

We have investigated the potential for laser operation of two sets of four-subband THz laser prototypes. This was
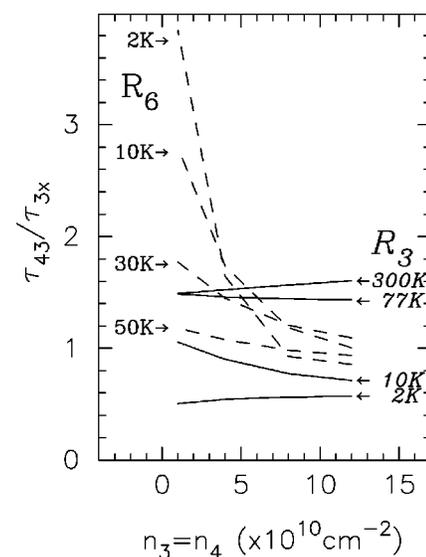

FIG. 7. Predicted population ratios for the R_6 (7.2 THz) and R_3 (11.7 THz) resonant prototypes listed in Table II. The electron densities are $\Sigma n_i = 50 \times 10^{10}$ cm^{-2}, and $n_2 = n_3 = n_4$. The dashed lines with nonitalic labels are for the R_6 prototype at a range of temperatures (2, 10, 30, and 50 K). The solid lines with italic labels are for the "room temperature" R_3 prototype at a range of temperatures (2, 10, 77, and 300 K).

ment is that rapid depopulation of the lower laser level by near-resonant LO-phonon scattering compensates for the strong 4131 electron–electron repopulation process. The largest population ratios (up to 4) are predicted for the prototypes emitting in the mid-THz range at low temperatures, but the most encouraging result is that those designed to emit at above 10 THz have population ratios significantly over 1 at *room temperature*. Furthermore, this room temperature inversion in the high-THz prototypes seems insensitive to increased optical excitation strength, which is not the case for the promising (low temperature) mid-THz prototypes. The relatively modest population ratios predicted for the high-THz prototypes may make achieving lasing in a practical device much harder. However, these results also show that it is not necessary to restrict designs to emission energies less than the LO-phonon energy in order to suppress $1/\tau_{43}$ relative to $1/\tau_{3x}$.

In addition, we discovered that the dominant electron–electron scattering rates (3121 and 4131) increased significantly with temperature, although in general it is the temperature dependence of the LO-phonon rates which has the greatest effect on the predicted population ratios. With this temperature dependence taken into account, the possibility of designing room temperature devices is more likely, with the higher frequency THz prototypes showing more promise.

[1] V. Berger, Semicond. Sci. Technol. **9**, 1493 (1994).

[2] F. H. Julien, A. Sa'ar, J. Wang, and J. P. Leburton, Electron. Lett. **31**, 838 (1995).

[3] F. H. Julien, Z. Moussa, P. Boucaud, Y. Lavon, A. Sa'ar, J. Wang, J.-P. Leburton, V. Berger, J. Nagle, and R. Planel, Superlattices Microstruct. **19**, 69 (1996).

[4] P. Harrison and R. W. Kelsall, J. Appl. Phys. **81**, 1 (1997).

[5] P. Kinsler, P. Harrison, and R. W. Kelsall, Phys. Rev. B **58**, 4771 (1998).

[6] P. Harrison, W. E. Hagston, and T. Stirner, Phys. Rev. B **47**, 16404 (1993).

[7] M. Lundstrom, *Fundamentals of Carrier Transport* (Addison-Wesley, Reading, MA, 1990).

[8] P. Kinsler, R. W. Kelsall, and P. Harrison, Physica B (to be published).

[9] P. Kinsler, R. W. Kelsall, and P. Harrison, Superlattices Microstruct. (to be published).

[10] B. K. Ridley, *Quantum Processes in Semiconductors* (Clarendon, Oxford, 1993).

[11] S. M. Goodnick and P. Lugli, Phys. Rev. B **37**, 2578 (1988).

[12] J. H. Smet, C. G. Fonstad, and Q. Hu, J. Appl. Phys. **79**, 9305 (1996).

[13] T. Ando, A. B. Fowler, and F. Stern, Rev. Mod. Phys. **54**, 437 (1982).

[14] P. F. Maldague, Surf. Sci. **73**, 296 (1978).

[15] Note that the $E_4 - E_3$ subband separation for the R_2 (10.7 THz) resonant prototype is 35.375 THz, about 0.6 meV lower than the LO phonon energy of 36 meV. This means that at the lowest temperatures (e.g., 2 K) most electrons do not quite have sufficient energy to emit an LO-phonon, so there is a distinct dip in the 2 K ph3x scattering rate in Fig. 5(a). This disappears at higher temperatures as the electrons gain extra (thermal) energy.